Analysis of measured stress data in a solid rocket motor

D.H. Smith* S.Y. Ho*

(Received 7 August 2000)

Abstract

A sinusoidal regression model is fitted to stress and temperature response data in a solid rocket motor under various thermal loading conditions. Using the model statistics and measured failure data, failure probability and reliability calculations are performed for each loading condition via two different approaches.

* WSD/DSTO, PO Box 1500, Salisbury SA 5108, Australia.

Contents

1 Introduction

Solid rocket motors in storage and service conditions experience dynamic thermal loading which, in combination with disparate thermal expansion properties of their constituent materials, induces time varying stress distributions in the propellant grain. Over a period of time such stresses can cause local structural failures with possible catastrophic launch consequences. In an aging rocket inventory the issue of service life thus becomes important, and the analysis described here constitutes the probabilistic component in a generic solid rocket motor service life program.

Probabilistic service life predictions for solid rockets has been given by Heller [1]. They employed linear elastic theory to calculate stress and temperature response as a function of input temperature in a concentric cylindrical geometry. Later improvements [2] incorporated propellant viscoelasticity, chemical aging and stress dependent cumulative damage. The following analysis is entirely based on measured stress and temperature response data from an instrumented solid rocket motor subjected to various thermal loading regimes, from benign magazine storage conditions to the aggressive high-amplitude temperature fluctuations of thermal cycling and shock.

The data is modelled by sinusoidal regression functions, with parameter estimates provided by Gauss-Newton iteration [3] and periodogram analysis. Probability density functions derived directly from the regression model are used to calculate failure probability by two different approaches, from which

corresponding reliability estimates are generated. Applicability of the sinusoidal model is also studied via some linear approximate diagnostic measures.

2 Modelling the Data

Temperature and stress response measurements at critical locations of the propellant grain [4] have yielded unevenly sampled time series data (t_j, X_j), $j = 1 \ldots N$, representing noisy output from a dynamical system. A vast array of techniques exists for the treatment of such data, including dynamic reconstruction procedures [5] and simpler nonlinear regression analysis [6], which models the data by an equation of the form

$$X_j = F(t_j, \theta) + \epsilon_j, \tag{1}$$

where $F(t_j, \theta)$ is a response function containing unknown parameters θ and the errors ϵ_j are independent, identically distributed (IID) random variables with zero-mean and constant variance. Under this description X_j becomes a random variable whose expected value is given by the response function at any time t_j. This latter approach will be applied here as a first step towards the ultimate goal of full dynamic reconstruction from arbitrarily spaced data.

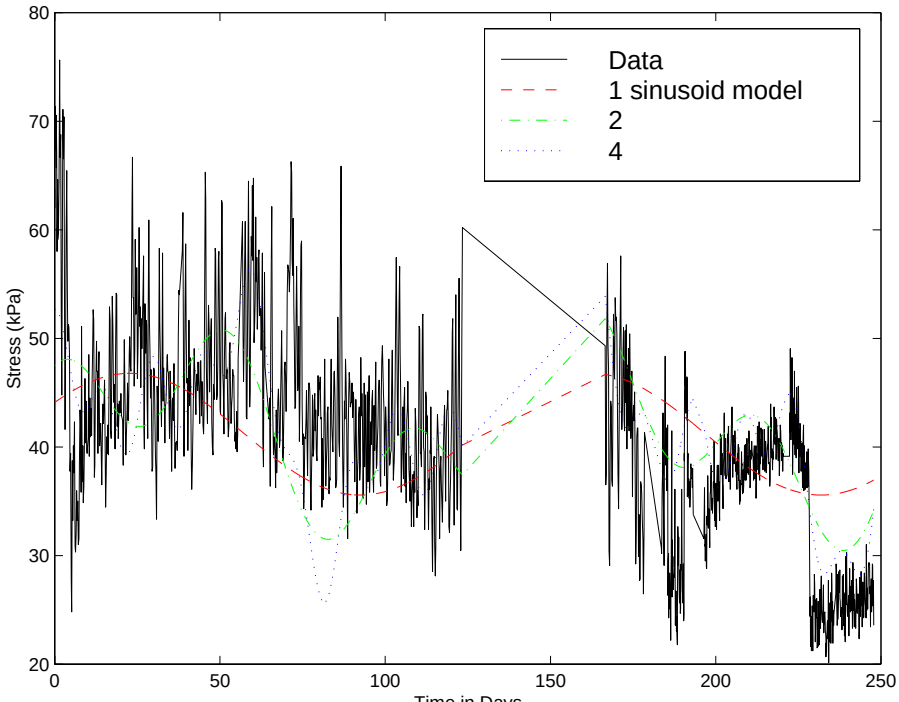

FIGURE 1: Sample stress response data under ambient aging conditions alongside regression model fits with various numbers of sinusoids.

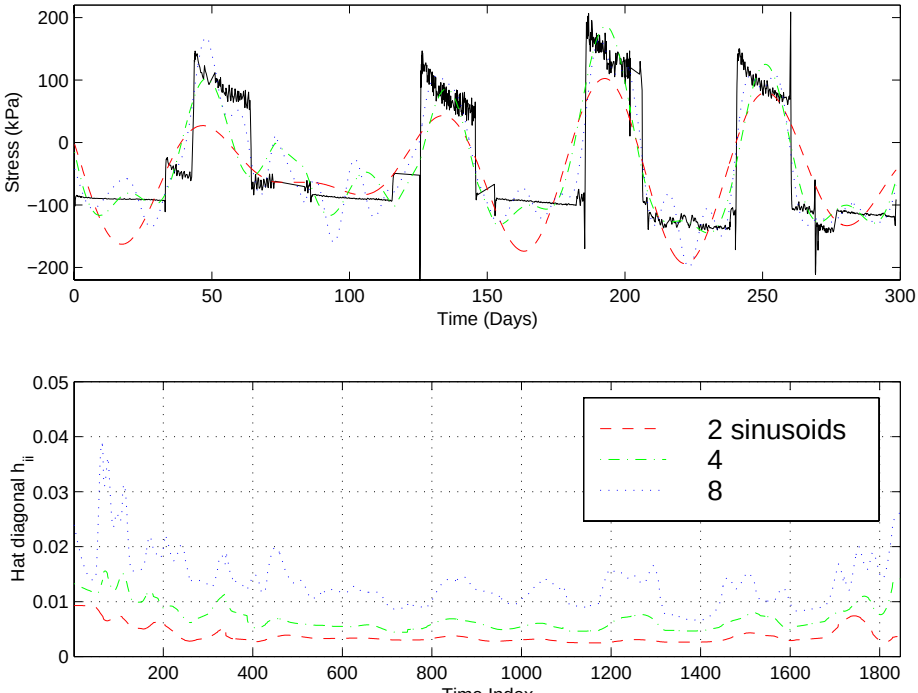

FIGURE 2: Thermal cycling stress data alongside various regression model fits. The lower plot gives corresponding diagonal hat matrix elements h_{ii}, which linearly approximate the deviation from non-constant variance present in the residuals. Higher oscillation in the residual variance estimates signals a warning against using too many model sinusoids.

2.1 A Sinusoidal Model

Sinusoids find wide applicability in physical systems as the solution of constant coefficient differential equations. On this basis the model response function will take the form

$$F(t,\theta) = X_0 + \sum_{k=1}^{K} A_k \cos(\omega_k t + \phi_k), \tag{2}$$

where the parameter vector θ contains a constant term X_0, amplitudes A_k, frequencies ω_k and phases ϕ_k. Similar models have been successfully used in a number of applications [7], and have proven superior to auto-regressive models in the long term prediction of sunspot activity [8].

2.2 Parameter Estimation

In this *non-Bayesian* approach the parameters are treated as unknown constants to be estimated from the data and as such are random variables themselves. Treating the model errors as normally distributed and applying the maximum likelihood criterion [6] requires minimisation of the function

$$f(\theta) = \sum_{j=1}^{N} \left[X_j - X_0 - \sum_{k=1}^{K} A_k \cos(\omega_k t_j + \phi_k) \right]^2 . \tag{3}$$

Rather than conduct a full nonlinear optimisation on (3) from the start, periodogram analysis is initially used to give approximate maximum likelihood frequency estimates [9]. This involves maximising the periodogram function

$$P_N(\omega) = \frac{1}{N}\left|\sum_{j=1}^{N}(X_j - \overline{X})\exp(i\omega t_j)\right|^2, \qquad \left(\overline{X} = \frac{1}{N}\sum_{j=1}^{N} X_j\right) \tag{4}$$

by using Newton iteration to locate zeros of $P'(\omega)$ in an appropriate frequency range defined by the temporal data length. Once a first frequency has been determined, additional components are obtained by a filtering procedure in which the periodogram is successively recomputed after removing a pure sinusoid at each frequency [10]. Given a set of frequencies, the remaining parameters are obtained by linear least squares on (3), with final refinement of the entire parameter set provided by Gauss-Newton iteration [3].

2.3 Sample Data Fits

Stress response data under ambient aging, representing controlled storage conditions with low amplitude temperature fluctuation, is given in Figure 1 along with regression model curves of 1, 2 and 4 sinusoidal components. None of the models offers adequate resolution of the high initial stresses for $t \leq 5$, an anomalous local minimum appears at $t \approx 80$ in the 2/4 curves, and poor resolution near $t = 250$ acts against the 1 component model. For thermal cycling, stress data is given in Figure 2 alongside model fits with 2,

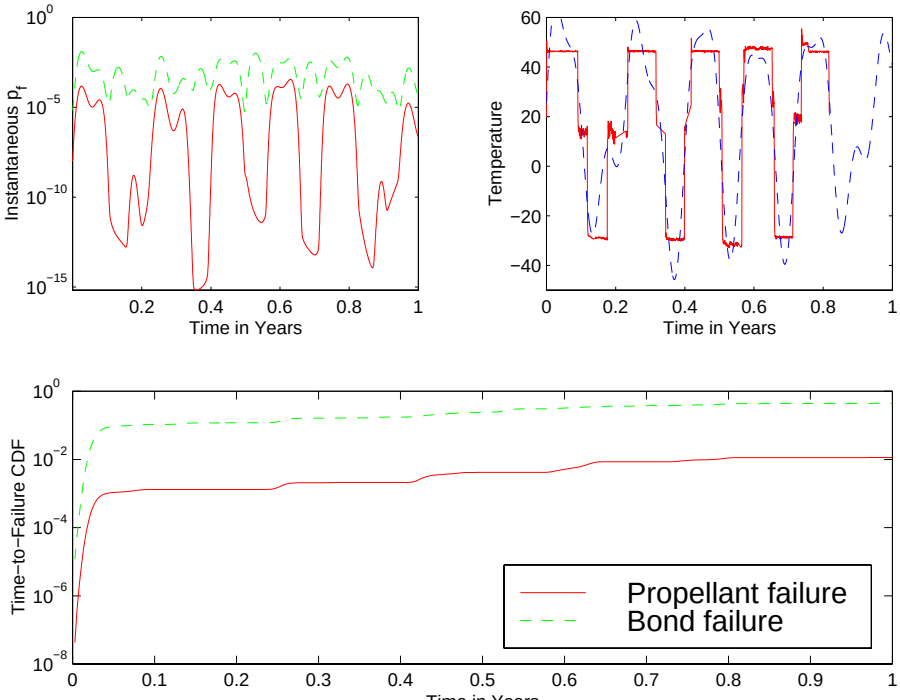

FIGURE 3: Comparison between propellant strength and propellant/inhibitor bond failure criteria under thermal cycling, using a 4 component regression and 64 point Laguerre quadrature. The latter criterion produces significantly higher failure probability during the cold cycle, displaying more consistency with experimental observations.

TABLE 1: Parameter estimates, standard errors and linearised 90% confidence intervals for thermal cycling stress data and a 2 component regression model.

Parameter	Estimate $\hat{\theta}_j$	Std Error.	90% linearised limits
X_0 (constant)	-46.1349	1.5148	$(-48.6286, -43.6411)$
A_1 (amplitude)	85.4911	2.2121	(81.8496,89.1326)
A_2 (amplitude)	65.6205	2.1904	(62.0147,69.2263)
ω_1 (frequency)	0.0945	0.0003	(0.0940,0.0950)
ω_2 (frequency)	0.1204	0.0004	(0.1197,0.1211)
ϕ_1 (phase)	0.8290	0.0558	(0.7371,0.9208)
ϕ_2 (phase)	1.7465	0.0757	(1.6218,1.8712)

4 and 8 sinusoidal components. Although the oscillatory features in the data have been captured, stress relaxation portions are not well resolved. The behaviour displayed in these plots immediately demands further analysis.

2.4 Regression Model Diagnostics

Inserting the parameter estimates $\hat{\theta}$ into the exact regression model (1) defines the residuals, $r_j = X_j - F(t_j, \hat{\theta})$, which do not inherit the IID properties of their exact model counterparts ϵ_j. Half normal quantile plots [11] give some positive evidence for residual normality but raise questions as the number of components is increased. Violations of constant variance and independence

are evident in the approximate residual covariance matrix [12]

$$\mathrm{cov}(\mathbf{r}) = \sigma^2(I - H),$$

where σ^2 is the true model error variance and the matrix $H = A^T(AA^T)^{-1}A$, with A containing the residual gradient vectors $A_{ij}(\theta) = \frac{\partial r_j}{\partial \theta_i}$. H is analogous to the hat matrix of linear regression [12] and is readily available as a by-product of the Gauss-Newton procedure. Diagonal hat matrix elements at the estimated parameter values are shown in Figure 2 for various model fits to a thermal cycling stress data sample. As more sinusoids are included in the model the curves rise and become more oscillatory, particularly near the ends of the time interval. Rising curves coincide with reduced residual variance as more model sinusoids are added and increased oscillation represents greater departures from non-constant variance.

Some statistical properties of the parameter estimates $\hat{\theta}$ can also be extracted by linearisation, in particular a measure of their precision. Linearly, the maximum likelihood parameter estimates are unbiased and the associated linear covariance matrix approximation is given by

$$\mathrm{cov}(\hat{\theta}) = E\left[(\hat{\theta} - \theta^*)(\hat{\theta} - \theta^*)^T\right] = \sigma^2(AA^T)^{-1},$$

in which the diagonal elements indicate mean squared parameter errors. Standard errors, which approximate the standard deviation of the parameters, are then generated by replacing σ^2 with the residual mean square [6], $s^2 = f(\hat{\theta})/(N-p)$, where p is the total number of model parameters. Corresponding approximate confidence intervals [13] are given in Table 1 for a two

component model fit to the thermal cycling stress data of Figure 2. For each parameter the standard errors are at least one order of magnitude smaller than the estimate, with frequency producing the lowest relative errors. Similar behaviour is observed on the same data with a four sinusoid model but an increase to eight components sees the appearance of some large amplitude discrepancies, with some errors exceeding three times the corresponding estimate. For the ambient aging temperature data, amplitude error anomalies start to appear in a four component model.

The above limited analysis has signalled clear warnings against the use of too many sinusoidal regression components. Further analysis incorporating nonlinearity is required to provide more insight into this behaviour.

3 Calculation of Failure Probability and Reliability

Time varying normal probability density functions for stress and temperature response, as provided by the regression model, must be supplemented with similar functions for the material strength in order to calculate failure probability. An experimental material characterisation program [4] has provided failure data, from which strength PDF's are formulated.

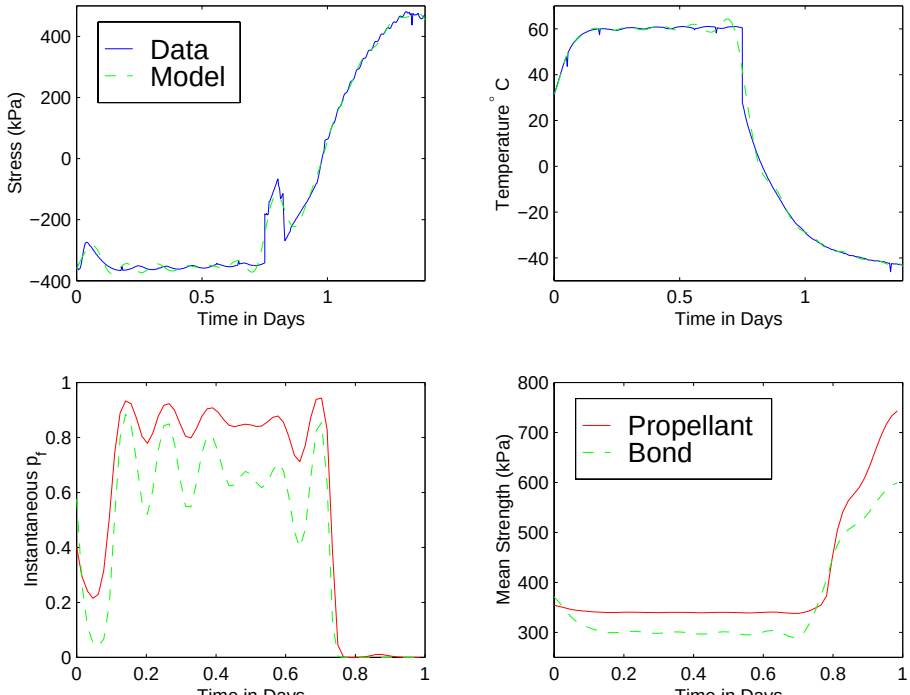

FIGURE 4: Thermal shock stress and temperature data for 1 cycle alongside regression model fits with 12 sinusoids. Computed instantaneous failure probability and predicted mean strength are given over a 1 day period in the lower plots, showing very high failure probability during the hot portion. This is in conflict with experimental observation and the absence of a cumulative damage mechanism in the current model may be partly responsible.

3.1 Strength Data and Statistical Characterisation

Table 2 gives strength data for failure by both uniaxial tension and propellant-inhibitor debonding. Time dependent probability density functions for the strength are constructed by treating these sample estimates as piecewise linear functions of temperature, which has previously been characterised as a normal random variable. The expected values of the strength mean and variance estimates are then evaluated by integration.

An appropriate strength distribution function is provided by the Weibull distribution [14], with a long history of application in strength of materials and failure studies. This has probability density function

$$f_S(S,t) = \frac{\alpha(t)}{\beta(t)} \left(\frac{S}{\beta(t)} \right)^{\alpha(t)-1} \exp\left[- \left(\frac{S}{\beta(t)} \right)^{\alpha(t)} \right], \quad S \geq 0, \tag{5}$$

where the parameters $\alpha(t)$ and $\beta(t)$ are related by a pair of nonlinear equations involving gamma functions. These can be easily solved by eliminating β and applying Newton iteration to the resulting equation for α.

3.2 Failure Probability by Direct Integration

Both tensile and compressive stress responses have been recorded in the data samples, and failure is deemed to occur when the absolute stress exceeds the

TABLE 2: Propellant and propellant-inhibitor bond strength data, representing sample mean values taken from unaged propellant specimens at each temperature. The error bounds represent two sample standard deviations.

Temperature ($°C$)	-40	20	60
Propellant strength (MPa)	0.84 ± 0.09	0.36 ± 0.05	0.34 ± 0.05
Bond strength (MPa)	0.65 ± 0.20	0.40 ± 0.05	0.31 ± 0.05

corresponding strength. Treating stress and strength as independent random variables, failure probability at any time, $p_f(t)$, is then defined by the stress-strength interference integral

$$p_f(t) = \int_0^\infty \int_0^y f_S(S,t)\, dS\, f_y(y,t)\, dy, \tag{6}$$

where y denotes the absolute stress, with probability density $f_y(y,t)$ derived from the stress PDF. Analytic evaluation of the inner integral leaves a semi infinite integral which is numerically evaluated by Laguerre quadrature [15], or the trapezoid rule. According to the Euler-Maclaurin error formula [15] the trapezoid rule provides exceptional accuracy in this case since the integrand is smooth with zero derivatives at the integration limits.

3.3 The Second Moment Method

For the case in which stress and strength are independent normally distributed variables, the failure probability becomes

$$p_f = 1 - \Phi\left(\frac{\mu_1 - \mu_2}{\sqrt{\sigma_1^2 + \sigma_2^2}}\right) = 1 - \Phi(\gamma), \tag{7}$$

where Φ is the standard normal distribution function and γ is the *safety index*, dependent only on the first two moments of stress and strength, μ_i and σ_i. γ is the minimum distance from the origin of reduced variables, $x_i' = (x_i - \mu_i)/\sigma_i$, to the failure line, and also coincides with the maximum likelihood point for the joint stress/strength distribution on this line.

Second moment methods [16] utilise only the first two moments for each design variable and work with *performance functions* whose sign indicates safety and danger regions within the design variable space. The failure surface is the zero contour of the performance function, and calculation of failure probability is a constrained minimisation problem. Non-normal design variates require transformation to equivalent normal variables before performing the minimisation, however this costly computational step can often be avoided with little penalty, as demonstrated by Shinozuka [17]. Locating the ML point of the original distributions by Newton iteration and then transforming the result back to normal variables before applying (7) gives a useful approximation for comparison with the direct integration results.

3.4 Calculation of Reliability

Given failure probability at any time from direct integration or the second moment approximation it is required to calculate the corresponding reliability $R(t)$ over a certain time period. A representative measure of daily failure probability p_j will be defined as the time-integrated mean value

$$p_j = \frac{1}{t_j - t_{j-1}} \int_{t_{j-1}}^{t_j} p_f(t)\, dt. \tag{8}$$

Reliability $R(n)$ at n days is defined as the probability of no failures occurring during this interval, $R(n) = \prod_{j=1}^{n}(1 - p_j)$. Alternatively, the cumulative distribution function for time to failure is defined as one minus the reliability.

4 Computed Results

Computed instantaneous failure probability and time-to-failure CDF curves for the various thermal loading regimes indicate service life expectancies for continual loading under each condition. Real service loading will comprise combinations from each regime, which is beyond the scope of this analysis.

4.1 Ambient Aging

Mean strength to mean stress ratios in the vicinity of 10 translate to very low failure probabilities in this benign loading regime. Calculations with regression models containing up to 8 sinusoidal components have demonstrated close agreement between direct integration by Laguerre/trapezoid quadrature and second moment results, with the latter approach proving more computationally expensive due to the Newton iterations required at each time step. After 10 years, the results indicate a probability of failure not exceeding 10^{-9}.

4.2 Thermal Cycling

This aggressive loading induces compressive and tensile stress responses as shown in Figure 2, with corresponding temperature response shown in Figure 3. Mean stresses reach considerably higher values than those seen in ambient aging and the temperature fluctuation induces large variations in mean strength. Using the maximum propellant stress as failure criterion produces high instantaneous failure probability during the hot cycle where mean strength is low, as calculated from a four component model with 64 point Laguerre quadrature and displayed alongside the temperature response in Figure 3. Also shown in this figure is the corresponding result for propellant/inhibitor bond failure, which features considerably less oscillation and several high failure probability regions during the cold cycle portion, partly due to a significantly lower bond strength at $-40°C$. Experimentally, failure

is expected during the cold cycle portion [4], which immediately suggests the latter failure criterion as the more appropriate. Time-to-failure CDF curves over the one year period are shown in Figure 3 for both failure criteria, indicating unacceptably high values after one year of sustained thermal cycling. Stress dependent cumulative damage, which has not yet been incorporated into the current model, is also expected to play an important role.

4.3 Thermal Shock

The most aggressive thermal loading regime features short duration cycles of less than one day between $55°C$ and $-40°C$. This is expected to be far more severe than any real service conditions and induces relatively rapid failure in the laboratory. Stress and temperature response data for the first of a series of cycles is shown in Figure 4 alongside regression model fits with twelve sinusoidal components. Considering both propellant strength and propellant/inhibitor bond strength produces very high instantaneous failure probability in the hot portion followed by a sudden decline, essentially following the mean strength behaviour, as shown in Figure 4, which gives computed results over one day. This conflicts with experimental results, in the sense that failure is observed during the cold portion [4], and indicates the need for further physical model refinement. As for thermal cycling, the effect of cumulative damage on this behaviour is of particular interest.

5 Summary and Conclusions

A sinusoidal regression model has been used to analyse measured stress and temperature response data at critical structural locations of a solid rocket motor subjected to various thermal loading regimes. Corresponding structural failure probability and its temporal evolution have been calculated from the model in conjunction with measured failure data. While the computed results show intuitive agreement with life expectancies under the given loading patterns, several important issues concerning the model fit have emerged. Resolution of stress relaxation regions is not entirely adequate with pure sinusoids and improvements will be sought by the incorporation of exponential damping terms. Another question demanding further attention involves the actual number of sinusoidal components to be used. Initial warnings against the use of too many components have been provided by linear diagnostic measures of the parameter and residual behaviour but further nonlinear analysis will be necessary to provide clearer answers. Stress-dependent cumulative damage also needs to be considered to provide a strength reduction mechanism.

This analysis represents a first step in probabilistic service life assessment from measured response data and will serve a useful purpose in the development of more elaborate techniques. Ultimately, full dynamic reconstruction will be sought, allowing studies of the response behaviour under any desired thermal loading profile.

References

[1] R.A. Heller, M.P. Kamat, and M.P. Singh. Probability of solid propellant motor failure due to environmental temperatures. *J. Spacecraft and Rockets*, 16:140–146, 1979. C1307

[2] R.A. Heller and M.P. Singh. Thermal storage life of solid-propellant motors. *J. Spacecraft and Rockets*, 20:144–149, 1983. C1307

[3] R. Fletcher. *Practical Methods of Optimization*. Wiley, 1987. C1307, C1312

[4] S.Y. Ho and P. Macdowell. New service life methodologies for solid propellant rocket motors. DSTO-RR-0099, 1998. C1308, C1316, C1323, C1323

[5] D. Coca and S.A. Billings. Continuous-time system identification for linear and nonlinear systems using wavelet decompositions. *International Journal of Bifurcations and Chaos*, 7:87–96, 1997. C1308

[6] G.A.F. Seber and C.J. Wild. Least squares. In J.L. Stanford and S.B. Vardeman, editors, *Statistical Methods for Physical Science*, Academic Press, 1994. C1308, C1311, C1315

[7] D.R. Brillinger. Fitting cosines: some procedures and some physical examples. In I.B. MacNeill and G.J. Humphrey, editors, *Applied*

Probability, Stochastic Processes and Sampling Theory, pages 75–100, Reidel, 1987. C1311

[8] E. Damsleth and E. Spjotvoll. Estimation of trigonometric components in time series. *J. American Stat. Assoc.*, 77:381–387, 1982. C1311

[9] A.M. Walker. On the estimation of a harmonic component in a time series with stationary independent residuals. *Biometrika*, 58:21–36, 1971. C1312

[10] J.H. Horne and S.L. Baliunas. A prescription for period analysis of unevenly sampled time series. *The Astro. J.*, 302:757–763, 1986. C1312

[11] M.B. Wilk and R. Gnanadesikan. Probability plotting methods for the analysis of data. *Biometrika*, 55:1–17, 1968. C1314

[12] G.J.S. Ross. *Nonlinear Estimation*. Springer-Verlag, New York, 1990. C1315, C1315

[13] D.A. Ratkowsky. *Handbook of Nonlinear Regression Models*. Marcel Dekker Inc., 1990. C1315

[14] W. Weibull. A statistical distribution function of wide applicability. *J. Applied Mechanics*, 18:293–297, 1951. C1318

[15] P.J. Davis and P. Rabinowitz. *Methods of Numerical Integration* Academic Press, Orlando, 1984. C1319, C1319

[16] A.H.S. Ang and W.H. Tang. *Probability Concepts in Engineering Planning and Design, Volume II.* Wiley, New York, 1984. C1320

[17] M. Shinozuka. Basic analysis of structural safety. *J. Structural Engineering*, 109:721–740, 1983. C1320